Proceedings of GT2006
ASME Turbo Expo 2006: Power for Land, Sea and Air
May 8-11, 2006, Barcelona, Spain

GT2006-90307

NUMERICAL SIMULATION OF THE FLOW INTERACTION BETWEEN TURBINE MAIN ANNULUS AND DISC CAVITIES

Jérôme Boudet*
LMFA
Ecole Centrale de Lyon
Ecully, 69134
France
Email: jerome.boudet@ec-lyon.fr

Nicholas J. Hills
John W. Chew
Thermo-Fluid Systems UTC
University of Surrey
Guildford, Surrey, GU2 7XH
United Kingdom

ABSTRACT

This paper presents numerical simulations of the unsteady flow interactions between the main annulus and the disc cavity for an axial turbine. The simulations show the influence of the main annulus asymmetries (vane wakes, blade potential effect), and the appearance of rim seal flow instabilities. The generation of secondary frequencies due to non-linear interactions is observed, and the possibility of further low frequency effects and resonance is noted. The computations are compared to experimental results, looking at tracer gas concentration and mass-flows. Results are further analysed to investigate the influence of the rim seal flow on the blading aerodynamics. The flow that is ejected through the rim seal influences the unsteady flow impinging the blades. The influence of this rim-seal flow is even observed downstream of the blades, where it distorts the radial profile of stagnation temperature.

NOMENCLATURE

d axial distance between the rows
f_{bld} blade passing frequency
Ma characteristic Mach number (based on U_e)
m_c coolant mass-flow
m_e main-inlet mass-flow
P pressure
Re_x Reynolds number (based on U_e and r_{hub})
r_{hub} hub radius
T temperature
U_c characteristic velocity based on m_c
U_e characteristic velocity based on m_e
x, r, θ cylindrical coordinates
x, y, z cartesian coordinates
β relative flow angle in the circumferential direction
η isentropic efficiency
φ sealing efficiency, based on the concentration of coolant flow
ψ mass-flow ratio through the rim seal (estimate of φ)
Π stagnation pressure ratio between main inlet and outlet
ρ_e characteristic density in the main annulus
CFD Computational Fluid Dynamics
0 [subscript] stagnation quantities
i and o [subscript] inlet and outlet
$\hat{}$ [superscript] Fourier transform
– [superscript] Time average

INTRODUCTION

The continuing drive to improve turbomachinery efficiency has led to both high turbine inlet temperatures and increasing interest in the aerodynamic effects of turbine rim seal flows. In axial flow turbines with shrouded blades and vanes there will be gaps between rotating and stationary sections on the annulus walls. These gaps must accommodate relative movement of

*Address all correspondence to this author.

the rotating and stationary components, and will allow flow exchange, at the inner annulus line, between the main annulus gas and the cavity between rotating and stationary discs. To avoid overheating of turbine discs, a positive flow of cooling air may be maintained through the rim seal gap, suppressing ingestion of hot annulus gas into the disc cavity. The level of sealing flow required and the spoiling effects of this flow in the annulus are of obvious interest. In lower pressure turbine stages, hot gas ingestion may not be of such concern, but the effects of interaction of cavity and annulus flows on performance remain important.

Much of the previous research on rim seal flows has concentrated on either ingestion or performance effects. For example, design methods and experimental correlations have been proposed for estimating ingestion due to disc pumping [1, 2]. As discussed by Boudet *et al.* [3], in the absence of a strong annulus flow (as is the case for inner seals) ingestion is driven solely by disc pumping. Axisymmetric, steady computational fluid dynamics (CFD) solutions do not capture this ingestion, but unsteady, 3D solutions give much better agreement with experimental measurements. CFD solutions reveal unsteady 3D flow in the seal region, even though the geometry and boundary conditions are steady and axisymmetric.

Further design methods and correlations have been derived for ingestion due to pressure asymmetries in the main annulus [4–7]. These inevitably involve simplifying assumptions, and neglect some of the complex flow interactions. More detailed analysis has been undertaken using CFD. Based on these studies and experimental data a number of workers have concluded that unsteady CFD models including both disc cavities and blading flow effects are required for a satisfactory physical description [5, 8–10]. Circumferential asymmetries due to either stationary or rotating blades can drive hot gas ingestion, and in the engine these combine producing unsteady flow. Interaction between the blade and vane flows may also be important. Recent CFD and experimental studies [3, 11–13] have shown that at low sealing flow rates unsteady flow features, unrelated to the blade passing frequency, are important and that complete 360 deg models may be required to fully represent these features. Flow structures similar to those identified for ingestion due to disc pumping have been identified in CFD solutions, and confirmed experimentally by unsteady pressure measurements. Such effects have now been observed for a number of different configurations. In some cases CFD results have indicated that ingestion due to disc pumping, as calculated in models without blades or vanes, is stronger than that due to the blade and vane pressure asymmetries.

As discussed by Rosic *et al.* [14], until relatively recently, rim seal leakage flows have usually been neglected or treated separately in CFD analyses of turbine performance. However, as shown by Rosic *et al.* [14] and Cherry *et al.* [15] a need for more detailed modelling of secondary flow path features, such as the disc cavities, has been recognised. In these studies cavity flows are included in steady multi-stage turbine models, with mixing planes used at interfaces between rotating and stationary components. Cherry *et al.* recommend further modelling of secondary flow paths as CFD capability improves in the future. Rosic *et al.* state that full calculation of leakage and cavity flows is needed to obtain good agreement with measurements.

In the present paper, unsteady CFD results are presented for a turbine stage, including blades, vanes, interdisc cavity and rim seal. This model corresponds to a test rig at the University of Sussex, with the particular rim seal geometry selected as measurements of mainstream gas ingestion had shown unexpected results. The next section presents the experimental configuration and the numerical approaches. The flow through the rim seal (ejection and ingestion) is analysed in the following section, with a particular focus on the different frequencies. Another section then considers the influence of the rim seal flow inside the main annulus. Finally, conclusions are drawn, together with perspectives for future work.

EXPERIMENTAL CONFIGURATION AND COMPUTATIONAL MODEL

The configuration consists of a turbine stage from the Gnome H1200 Power Turbine Module, with 26 vanes and 59 blades. A cavity is located between the static and the rotating discs ($r \leq r_{hub}$), and it is separated into three different sections that are superposed in the radial direction. The rim seal is of chute type, and the coolant flow enters the main annulus with an oblique angle towards the downstream direction. This geometry is representative of industrial design, used to limit ingestion of hot gas inside the cavity. Measurements have been carried out by Gentilhomme *et al.* [9, 16] at the University of Sussex, and are used for comparison with the present computations.

Figure 1 presents the central part of the computational domains. The static domain contains one vane passage and the cavity. Only the outer two sections of the cavity are modelled. The chute rim seal can be observed, with an oblique angle directing the coolant flow in the streamwise direction when entering the main annulus. The rotating domain contains two blade passages, and moves in the negative θ-direction (opposite to the arrow in Fig. 1). A sliding plane is located inside the main annulus, just downstream of the rim seal, to exchange unsteady flow information between the static and rotating frames of reference. The sliding plane can be seen in Fig. 1: the striped faces correspond to the static domain outlet and the rotating domain inlet. Finally, periodicity is used on the sides of the domains to represent the full circumference. Computations are carried out using *Hydra* [17], a finite volume solver using unstructured meshes. The Reynolds-Averaged Navier-Stokes (RANS) equations are applied with the Spalart-Allmaras turbulence model [18]. An advection-diffusion equation was also implemented to represent the distribution of a passive scalar. Spatial discretization uses 2^{nd} order centred schemes, with a 2^{nd} order smoothing (1^{st} order

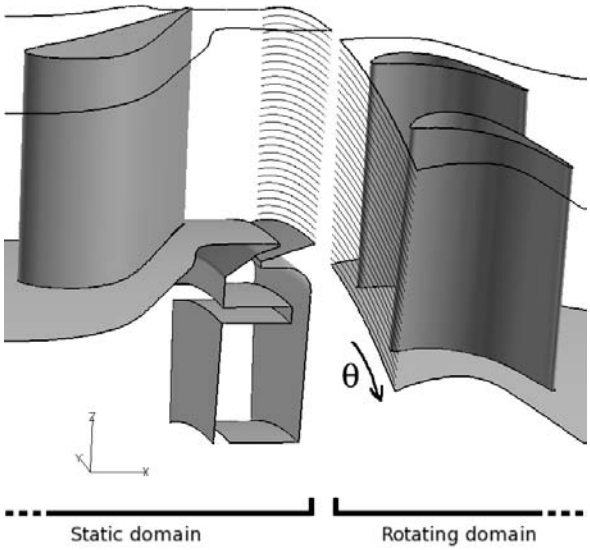

Figure 1. CENTRAL PART OF THE COMPUTATIONAL DOMAINS (THE MAIN INLET AND OUTLET DUCTS ARE NOT SHOWN). MAIN FLOW DIRECTION IS FROM LEFT TO RIGHT. THE STRIPED FACES AT THE STATIC DOMAIN OUTLET AND ROTATING DOMAIN INLET CORRESPOND TO THE SLIDING PLANE.

around the shocks). Time formulation is implicit, with 100 time steps per sliding period of the domain ($1/27^{th}$ of disc rotation), corresponding to time steps around 3×10^{-6} s. Dual time stepping is used for inner iterations, with $CFL = 2$ (Courant number). Characteristic convection times are very different between the main annulus and the cavity. For a similar length scale, axial velocity is about ten times higher inside the main annulus than radial velocity inside the cavity. Resolution of main annulus unsteadynesses requires 100 time steps per sliding period of the domain, but hundreds of periods are then required to reach unsteady convergence inside the cavity. This makes these computations particularly expensive. Post-processings (including averages) are then carried-out over the period corresponding to the smallest aerodynamic frequency. Figure 2 presents the computational grid, covering one vane passage, two blade passages and the upper two sections of the cavity. In the picture, S is a cutting surface through the bottom of the rim seal. It is used to calculate ψ, which estimates ingestion of main annulus gas into the cavity. Another grid, with a much denser mesh in the region around the rim seal, gave no major difference with the original grid during tests at two different operating conditions.

Concerning the boundary conditions, the main-annulus inlet is located on the left of views (a) and (c) in Fig. 2. The coolant inlet corresponds to the clearance of a fin attached to the rotor disc inside the cavity, and is represented by a slot on the bottom surface of the cavity (20% of the cavity width). At these boundaries, a subsonic inflow condition imposes the stagnation pressure, stagnation temperature, and flow angles. Static pressure is specified at the main annulus outlet, located on the right of views (a) and (c). The walls are represented by a no-slip condition, with wall functions for the turbulence model. The cell height at the wall lies in the range $15 \leq y^+ \leq 80$ (in wall units). Finally, periodicity is applied on the sides of the domain. The numbers of vanes and blades have been modified to 27:54 for the computations, in order to reduce the domain to 1 vane passage and 2 blade passages.

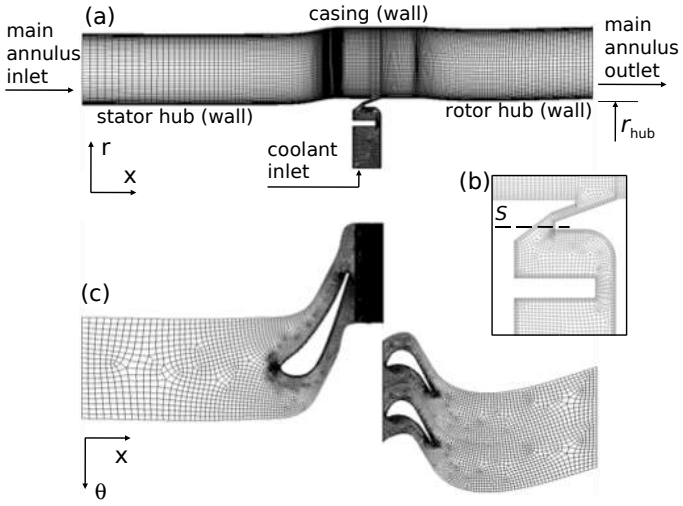

Figure 2. COMPUTATIONAL GRID. (a): SIDE VIEW, (b): CLOSE-UP VIEW OF THE RIM SEAL, (c): UPPER VIEW. $\theta = 0$ DEG CORRESPONDS TO THE VANE TRAILING EDGE.

The operating conditions are presented in Table 1 for the computations and the corresponding experiments from Gentilhomme *et al.* [9, 16]. The reference names are composed of the turbine operating condition (Design or OffDesign, according to the rotational speed), plus '1' for a low coolant mass-flow or '2' for a medium coolant mass flow. OffDesign1 and Design1 are compared to extract the influence of turbine operating condition, for similar coolant to mainstream velocity ratio. On the other hand, the comparison of Design1 and Design2 gives information about the influence of the coolant mass-flow, for the same operating condition (design). m_e is the main outlet mass flow, used to calculate the characteristic axial velocity U_e inside the main annulus. To obtain U_e, m_e is divided by the main-annulus constant section and a characteristic density (ρ_e, obtained with the perfect gas equation from pressure and temperature probe data between the two rows). Π is the stagnation pressure ratio of the turbine stage. For the computations, it is obtained from a plane just upstream of the vanes and a plane just downstream

Table 1. OPERATING CONDITIONS.

Computations

	m_e(kg/s)	Π	Ma	Re_x	U_c/U_e
OffDesign1	1.29	1.13	0.38	$3.54\times10^{+5}$	0.0808
Design1	4.47	2.13	0.97	$1.13\times10^{+6}$	0.0746
Design2	4.45	2.12	0.96	$1.12\times10^{+6}$	0.1250

Experiments

	m_e(kg/s)	Π	Ma	Re_x	U_c/U_e
OffDesign1	1.35	1.15	0.40	$3.85\times10^{+5}$	0.0838
Design1	4.58	2.49	0.92	$1.31\times10^{+6}$	0.0913
Design2	4.57	2.48	0.92	$1.31\times10^{+6}$	0.1170

of the blades, applying a mass-average. In the experiment, Gentilhomme [16] used local probe data upstream and downstream of the vanes. Ma is the Mach number obtained from U_e and the characteristic temperature measured between the two rows, and divided by $\cos(70\,\text{deg})$ to account for the geometrical deviation by the vanes (U_e is an axial velocity). The axial Reynolds number Re_x is calculated from U_e, the hub radius, and the characteristic main-annulus pressure and temperature between the two rows (estimate of density ρ_e with the perfect gas equation and estimate of viscosity with Sutherland's law). Finally, U_c is obtained by dividing the coolant inlet mass flow by the rim seal section and a characteristic density (obtained with the perfect gas equation from pressure and temperature probe data inside the cavity). The level of coolant flow is given by U_c/U_e, wich is a particularly representative parameter when comparing different operating conditions (cf. Gentilhomme [16]). On this academic rig, main inlet stagnation temperature is just around 380 K, and the coolant temperature is around 350 K at the radius of the computational coolant inlet. As observed in Table 1, operating conditions achieved in the computations do not exactly match the experiments. Adjustments could be done on the boundary conditions to compare more closely. However, taking into account the long computational time required by these unsteady computations, such adjustements were not done. Operating conditions are comparable, and the remaining discrepancies can be kept in mind for interpretation.

FLOW THROUGH THE RIM SEAL

Considering the disc cavity, radially outward flow in the rotor boundary layer is produced by the centrifugal force. This is compensated by the opposite movement in the stator boundary layer, as observed in the experiment of Batchelor [19]. When the coolant mass-flow is sufficient at the bottom of the cavity, this reduces the pumping effect in the stator boundary layer and there is no ingestion through the rim seal. But when the coolant flow is reduced, gas is ingested from the main annulus to feed the stator boundary layer. This has been already discussed in comparison with the experiments in a previous article by Boudet *et al.* [3], but the present paper focuses on further investigation and results.

Figure 3 presents three different snapshots of the flow inside the rim seal, for computation Design1. These snapshots are not a time sequence, but just representative instants. Actually, it is particularly difficult to find a periodic sequence. Fourier analysis will give more quantitative information. At the first instant, pressure is low at the outlet of the rim seal, and flow is ejected into the main annulus. At the second instant, pressure is higher inside the main annulus, because of a blade located downstream at the same angle. This drives flow into the cavity, through the rim seal near the rotor hub. The ingested flow counters the gas that is still ejected near the stator hub, generating a shear zone and vorticity. Finally, at the last instant, the ingestion is fully established and covers the whole section of the rim seal. This sequence clearly shows the influence of the potential field of the blades on the rim seal flow. The influence of the vanes is not further analysed here, because they are much farther from the rim seal than the blades (cf. Fig. 1).

Table 2 presents the level of ingestion inside the cavity, for both the computations and the experiments. In the experiments, tracer gas is fed at the coolant inlet, and its normalized concentration inside the cavity ($\varphi \in [0,1]$) is defined as the sealing efficiency. Here the steady value (time average) is measured on the stator at $r/r_{hub} = 0.96$ and $\theta = 0\,\text{deg}$. Considering the results, the strongest ingestion (i.e. lowest φ) is obtained at design condition for the lowest coolant flow rate (Design1). As expected, ingestion is reduced by increasing the coolant mass-flow (cf. Design2). More surprisingly, it is also reduced at off-design condition (cf. OffDesign1). In contrast, experimental results for different seal arrangements showed closer agreement between design and off-design conditions (Gentilhomme [16]). In the computations, the tracer gas is represented by a passive scalar, but only results for Design1 are available. A strong underestimate is shown, compared to the experiment. This underestimate has been discussed in other publications. CFD solutions for larger angular sectors (eg. 120 deg in reference [3]) have shown higher levels of ingestion even when vanes and blades are not modelled. There is also a possibility that inlet flow asymmetries lead to the higher ingestion levels in the experiment.

As detailed for example in reference [3], another quantity (ψ) is often used to approximate φ. The mass-flow ratio through

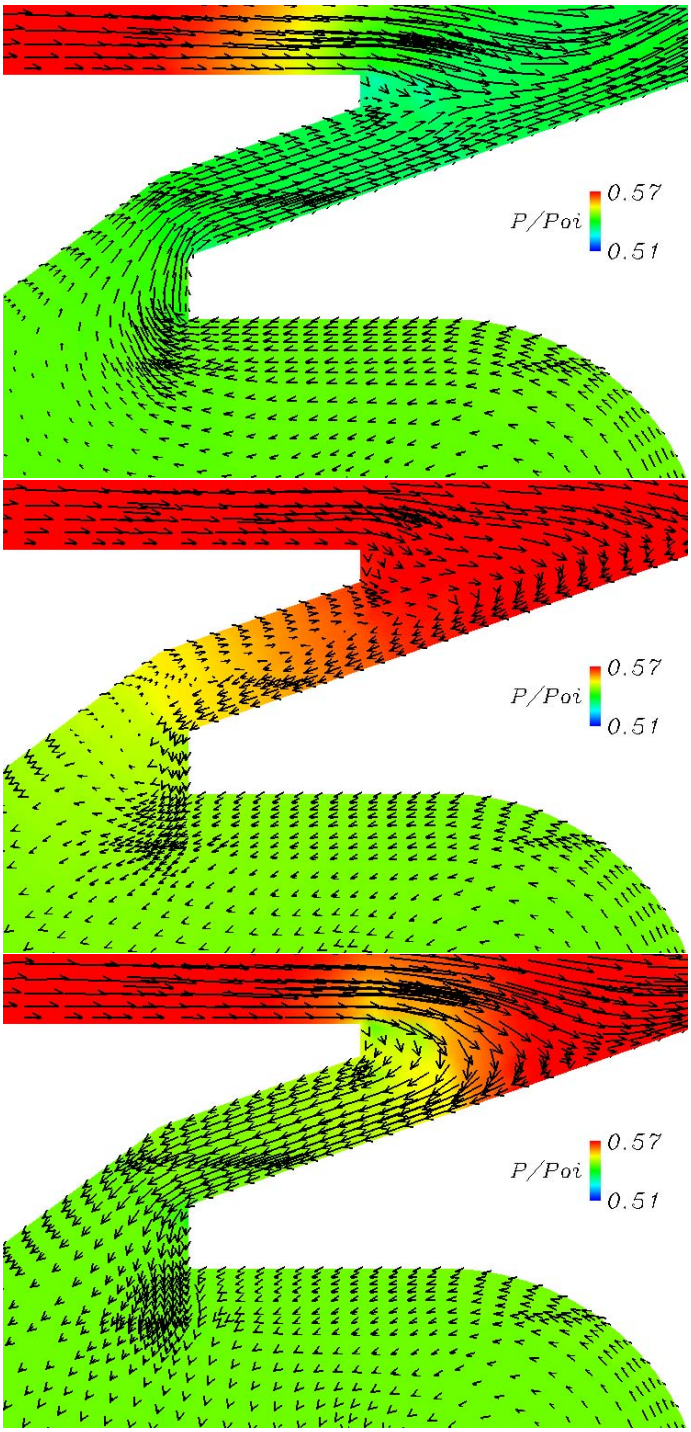

Figure 3. SNAPSHOTS PRESENTING CONTOURS OF PRESSURE AND ABSOLUTE VELOCITY VECTORS AT $\theta = 0$ deg INSIDE THE RIM SEAL, FOR COMPUTATION Design1.

Table 2. INGESTION.

	comput. φ	comput. ψ	exp. φ
OffDesign1	–	0.96	0.76
Design1	0.95	0.72	0.60
Design2	–	0.99	0.75

the rim seal is defined by: $\psi = 1 - \overline{m_{in}}/\overline{m_{out}}$, where m_{in} and m_{out} are the inward and outward mass-flows through the rim seal. The cutting surface S used to calculate m_{in} and m_{out} is located in the inner part of the rim seal, as shown in Fig. 2. ψ was extracted for the three computations, and the tendencies between the computations can be analysed, contrary to φ that is only available for computation Design1. Results are given in Table 2. It is interesting to note that the same tendencies are observed between the computed values of ψ and the experimental values of φ. ψ shows the increase of inward flow at Design1 compared to Design2 or OffDesign1. As shown above, the flow oscillates inside the rim seal, but it appears that only a limited amount of main-annulus gas enters the cavity. This explains why the correct tendencies are captured by ψ but φ remains high for computation Design1. As a conclusion, it is interesting to note that the experimental trends are correctly captured, even if ingestion is globally underestimated.

Unsteady pressure is extracted from numerical probes inside the cavity, on the stator disc surface at the same angular position as the trailing edge of the vanes. For computations OffDesign1 and Design2, only the blade passing frequency is visible: the rotation of the blades is the only source of unsteadiness. But for Design1, as illustrated in Fig. 4, other frequencies appear aside f_{bld}: at $f/f_{bld} = 0.12, 0.44$ and 0.56. A computation on the isolated cavity (no vane and no blade), presented in reference [3], shows that this is an instability that develops inside the cavity at a frequency similar to $f/f_{bld} = 0.44$. The other frequencies in the present computation can result from non-linear combinations between f_{bld} and the instability at $f/f_{bld} = 0.44$: $0.56 = 1.00 - 0.44$ and $0.12 = 0.56 - 0.44$. These different frequencies explain the difficulty to find a period when considering the snapshots of the rim seal flow (Fig. 3).

To investigate the spatial distribution of the frequencies, a second run was launched for Design1, extracting the Fourier transforms at $f/f_{bld} = 0.12, 0.44, 0.56$, and 1.00 during the computation, over the whole domain. When looking at the radial velocity, the largest amplitudes are obtained at $f/f_{bld} = 0.44$. This component, corresponding to the instability, is located inside the rim seal, as presented in Fig. 5 (top) for pressure. Con-

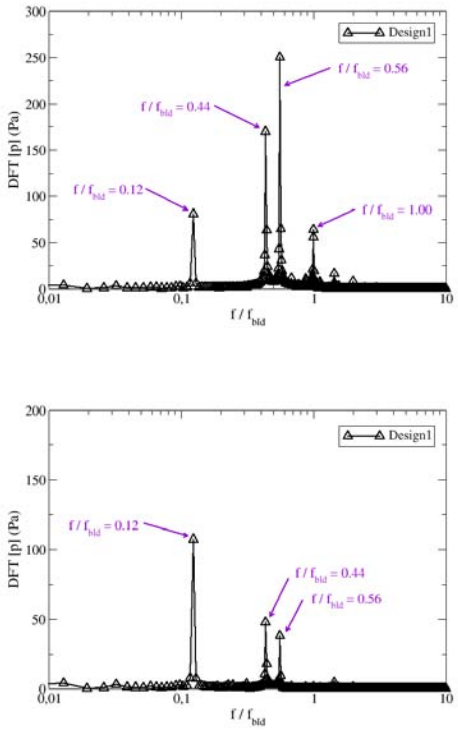

Figure 4. DISCRETE FOURIER TRANSFORM OF PRESSURE INSIDE THE CAVITY FOR COMPUTATION Design1 (TOP: AT $r/r_{hub} = 0.96$, BOTTOM: AT $r/r_{hub} = 0.88$).

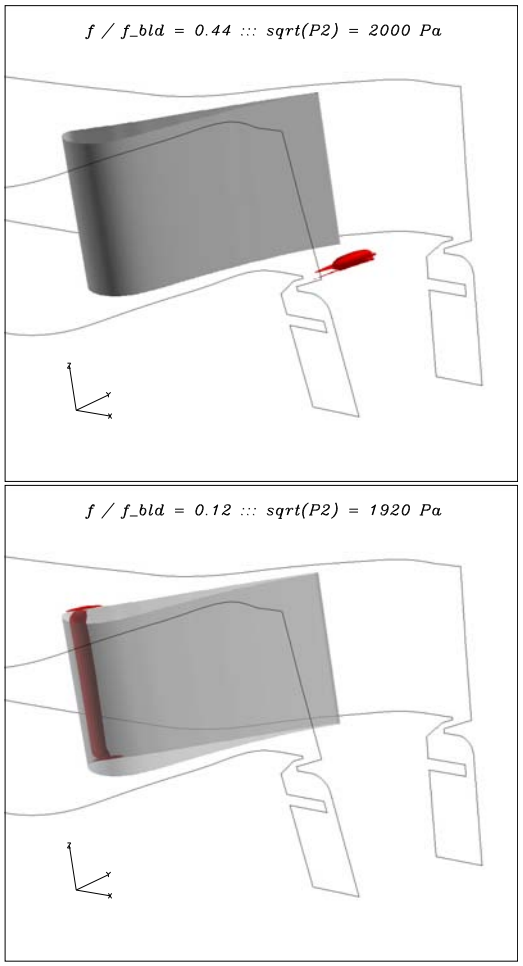

Figure 5. ISO-SURFACE OF FLUCTUATING PRESSURE AMPLITUDE AROUND THE VANE AND INSIDE THE CAVITY FOR COMPUTATION Design1 (TOP: $|\hat{P}| = 0.174 \times (1/2\rho_e U_e^2)$ AT $f/f_{bld} = 0.44$, BOTTOM: $|\hat{P}| = 0.167 \times (1/2\rho_e U_e^2)$ AT $f/f_{bld} = 0.12$, WHERE DENSITY ρ IS CALCULATED WITH THE PERFECT GAS EQUATION FROM LOCAL PRESSURE AND TEMPERATURE BETWEEN THE ROWS IN THE MAIN ANNULUS). THE ISO-SURFACE IS REPRESENTED IN DARK RED, AND THE VANE IS TRANSPARENT IN THE BOTTOM VIEW.

sidering again Fig. 4, it is worth noting that even though the dominant frequencies are $f/f_{bld} = 0.44$ and 0.56 at $r/r_{hub} = 0.96$ (near the rim seal), $f/f_{bld} = 0.12$ propagates more efficiently down to $r/r_{hub} = 0.88$. In Fig. 5 (bottom), the influence of $f/f_{bld} = 0.12$ is observed up to the leading edge of the vane. These fluctuations are located on the pressure side and the velocity vectors show no separation. Also, this is not an acoustic propagation from the rim seal because amplitudes are much stronger at the leading edge than inside the rim seal. The fluctuations near the vane leading edge could be due to small movements of the stagnation point, which focuses the most intense spatial variation of pressure. An unsteady blockage effect, generated by the rim seal flow, could create this movement of the vane stagnation point. The frequency at 12 % of the blade passing frequency can be particularly effective in influencing the flow through the main annulus, compared to the higher frequencies.

As shown for computation Design1, the fluctuations associated to the instability are mainly located inside the rim seal. In this region, at low coolant flow rate, the flow is governed by the competition between the centrifugal force and the pressure gradient. This is the condition for a Taylor-Couette instability. In a computation at Design1 operating condition, but without vanes and blades, Boudet *et al.* [3] isolated the corresponding zones of ejection and ingestion that alternate around the circumference. The circumferential extent of the domain was 120 deg in order to reduce the influence of the periodic boundary conditions on the natural period of the instability. Taylor-Couette instability is similar to Rayleigh-Bénard instability, and can be expected in very turbulent conditions (cf. Chavanne *et al.* [20]). Finally, when coolant flow is increased, instability is suppressed by the dominant centrifugal flow. Indeed, there is an instability at Design1 but not at Design2. This also happens at the off-design condition.

A computation (not presented here) was carried-out at off-design condition with a very low coolant flow rate ($U_c/U_e = 0.0455$) to force ingestion ($\psi = 0.76$), and a rim seal flow instability was observed. But when considering OffDesign1, rim seal flow is purely centrifugal and there is no instability.

The different frequencies obtained by non-linear combinations can have different effects. Here, $f/f_{bld} = 0.12$ propagates more efficiently through the domain. It could also affect ingestion, with low frequency velocity fluctuations being more effective in driving flow from the annulus into the cavity. Also, some frequencies could correspond to a resonance of the cavity and increase the fluctuating mass-flow through the rim seal.

INFLUENCE OF THE SEALING FLOW INSIDE THE MAIN ANNULUS

This section focuses on the perturbation of the main-annulus flow by the rim seal flow. The net flow ejected from the cavity is controlled by the coolant mass-flow imposed at the bottom of the cavity (cf. U_c/U_e in Table 1). This major parameter is correctly set in the computations, which supports the present analysis of the main-annulus perturbation. However, the net flow through the rim seal is composed of ejected flow (dominant because of the positive coolant flow) minus some ingested flow. As shown in the previous paragraphs, the ingested flow is underestimated, but respects the experimental tendencies when varying the coolant mass-flow. As a summary, the major influence of the net flow is captured, but the influence of ingestion is underestimated. This is a limitation of the present study.

Table 3 presents the isentropic efficiency, calculated from the computations using Eq. (1):

$$\eta = \frac{1 - < T_{0o} > / < T_{0i} >}{1 - (< P_{0o} > / < P_{0i} >)^{\gamma - 1/\gamma}} \qquad (1)$$

where the stagnation pressure and temperature are averaged on the surfaces and in time, weighted by the mass flow. For a given quantity Q ($= P_{0i}, P_{0o}, T_{0i}$ or T_{0o}):

$$< Q >= \frac{\int_t \int_S \rho Q \mathbf{v}.\mathbf{dS} dt}{\int_t \int_{S_i} \rho \mathbf{v}.\mathbf{dS} dt} \qquad (2)$$

where S is the considered surface (inlet or outlet surface). The inlet surface is composed of a cutting plane at $0.20\,d$ upstream of the vane leading edge, plus the coolant inlet. The outlet surface is a cutting plane at $0.12\,d$ downstream of the blade trailing edge. d is the axial distance between the vane trailing edge and the blade leading edge, at the hub.

Table 3. COMPUTED EFFICIENCY.

	η
OffDesign1	0.5354
Design1	0.8890
Design2	0.8876

As an estimate of the efficiency precision, the mass-flow error is calculated between the same inlet and outlet surfaces. This conservation measure is particularly interesting, because of the mass-averaged stagnation quantities used to calculate η. This estimate uses the averaged mass-flows evaluated during the efficiency calculation: this measures the precision of the solver, but also the precision of the processing technique (including the interpolations on the cutting planes). For the three computations, the mass-flow error lies within 0.19%. This value is not negligible for efficiency, and it will be taken into account for the analysis.

Efficiencies around 0.89 are obtained at design condition, in agreement with design expectations. In comparison, a very low value is calculated at off-design condition, around 0.54. This is related to a separation on the blade suction side, close to the tip, at off-design condition. The validity of this phenomenon is not further investigated, because the present study focuses on the region of the rim seal. Moreover, the off-design condition is not used in this section, which considers the influence of the two different coolant mass-flows used at design condition. Finally, it can be pointed out that the proper simulation of the blade tip region would require representation of the tip clearance.

It is then interesting to consider the influence of the coolant flow rate on the efficiency, for a given operating condition (design). Moving from Design1 to Design2, η decreases by 0.0014 (-0.15%). This variation is of the same order as the precision range. The efficiency can be expected to be reduced when increasing the coolant mass-flow, because of:

(i) The increase of the flow rate going through the cavity. Indeed, the elementary design of the cavity results in a poorer efficiency than in the main annulus. Consequently, the higher the mass-flow through the cavity, the lower should be the efficiency of the turbine.

(ii) The perturbation of the main-annulus flow by the ejection of more coolant gas through the rim seal.

The coolant mass-flow is increased by 0.20% of the total inlet mass-flow, and a variation of the same order can be expected for the efficiency because of point (i) alone. This lies within the precision range. Because the global variation of the efficiency lies also in the precision range, the influence of point (ii) is also within the precision range.

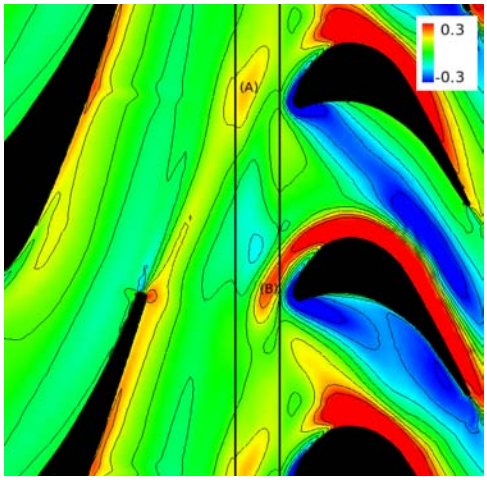

Figure 6. RADIAL VELOCITY (NORMALIZED BY U_e) AT 1 mm ABOVE THE HUB RADIUS, FOR COMPUTATION Design2. THE VERTICAL BLACK LINES REPRESENT THE RIM SEAL CLEARANCE AT HUB.

The local perturbation of the flow field is then investigated, keeping in mind the limited influence on the efficiency. Figure 6 presents the instantaneous radial velocity at 1 mm above the hub radius, for computation Design2 (higher coolant mass-flow). Centrifugal flow is shown on the suction sides, and centripetal flow on the pressure sides. This effect is particularly important for the blades. However, the centrifugal flow in the vane wake is shown to favour ejection through the rim seal (zone A). In zone B, flow ejected through the rim seal is shown to feed the centrifugal flow on the suction side of a blade. Finally, the expected blade-to-blade convection from the pressure side to the suction side is observed.

Figure 7 presents the envelope of the relative flow angle fluctuations, at a fixed angular position just upstream of the rotating row. The angular position corresponds to the vane trailing edge, but the axial position is just 1.8 mm upstream of the blade leading edges (11.7 mm downstream of the vane trailing edges). This location is not in the mean wake of the vanes, but the potential effect of the rotating blades deviates the wakes up to this point during limited periods of time. For both conditions, similar results are obtained over nearly the whole height (except in the hub region), with a fluctuation range around 20 deg. These fluctuations are due to the potential effect of the rotating blades. More interesting behaviours appear near the hub radius. For both conditions the sealing flow creates a broadening of the envelope. This hub region is about twice the width for Design2 than for Design1, covering about 12 % of the annulus height for Design2. At 6 % above the hub radius, the envelope is nearly 50 deg wide for Design2, compared to 20 deg for Design1. The influence of the rim seal flow on the relative flow angle can be explained by the lower angular moment of the flow coming from the cavity. The flow inside the cavity is only put in rotation by the friction of the rotor disc on one side, while the vanes impose strong swirl to the flow in the main annulus. For Design2, the stronger net-flow through the rim seal imposes stronger perturbations, over a wider zone of penetration. In comparison, the multiple frequencies and the oscillating rim-seal flow observed in Design1 do not have a strong influence here. However, it was shown that ingestion is underestimated, so the influence of this second parameter is not representative.

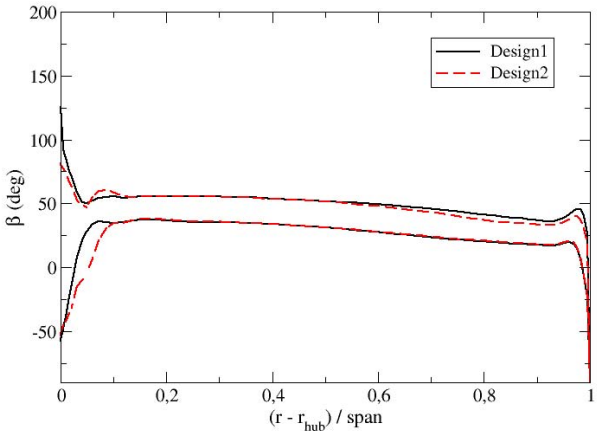

Figure 7. FLOW ANGLE ENVELOPE AT A FIXED ANGULAR POSITION JUST UPSTREAM OF THE ROTATING ROW. $x = x_{rotorLE} - 1.8$ mm and $\theta = \theta_{statorTE}$

Finally, Fig. 8 presents the radial distribution of stagnation temperature at $x = 68.36 \times 10^{-3}$ m (45.95×10^{-3} m downstream of the blade trailing edge). This profile is circumferentially and temporally averaged, and T_{0i} is the mass-averaged stagnation temperature that is calculated on the main and coolant inlets together. Differences are again limited between Design1 and Design2. However, a stronger distorsion of the profile appears for the case with higher m_c. The low-energy flow coming from the coolant inlet reduces the stagnation temperature near the hub, whereas it is increased near the casing. This effect is observed at more than two blade chord lengths downstream of the blades, and would have cumulative effects in the following stages of a turbomachine, perturbing the radial repartition of the load.

CONCLUSION

This paper presented a numerical investigation of the flow between the main annulus of a turbine stage and a disc cavity, in comparison with available experimental data.

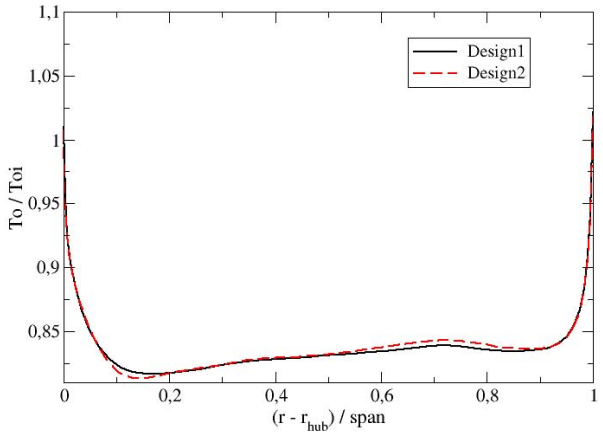

Figure 8. RADIAL PROFILE OF STAGNATION TEMPERATURE AT $x = 68.36 \times 10^{-3}$ m (CIRCUMFERENTIALLY AND TEMPORALLY AVERAGED).

First, the unsteady flow has been studied inside the cavity and through the rim seal. Different frequencies are shown to appear, due to the non-linear coupling between the blade passing frequency and an instability that develops inside the rim seal. Low frequencies are particularly hilighted, because of their ability to propagate through the domain. Concerning the ingestion of main-annulus gas inside the cavity, the trends are captured by the simulation when modifying the operating conditions, but the global level remains underestimated.

Second, the influence of the rim-seal flow inside the main annulus is analysed. The stronger the coolant flow, the stronger the perturbation of the flow angle upstream of the blades. The influence is also observed downstream of the blades, where the profile of stagnation temperature is perturbed.

While the influence of the unsteady flow effects on ingestion are clearly important, the current calculations show a limited influence of the rim seal flow on turbine performance. Further investigations are planned to clarify and extend there results. This will include full 360 deg unsteady modelling and use of large-eddy simulation to investigate the effects of turbulence in the rim seal flow.

ACKNOWLEDGMENT

The authors thank the DTI and the EPSRC for their support to the PUMA DARP project. Rolls-Royce plc is also acknowledged for the exchange of data, software and knowledge, and for its support to the TFS-UTC.

REFERENCES

[1] Bayley, F. J., and Owen, J. M., 1970. "The fluid dynamics of a shrouded disk system with a radial outflow of coolant". *Journal of Engineering for Power (transactions of the ASME),* **92**, pp. 335–341.

[2] Chew, J. W., 1989. "A theoretical study of ingress for shrouded rotating disc systems with radial outflow". *ASME Journal of Turbomachinery,* **113**, pp. 91–97.

[3] Boudet, J., Autef, V. N. D., Chew, J. W., Hills, N. J., and Gentilhomme, O., 2005. "Numerical simulation of rim seal flows in axial turbines". *Aeronautical Journal,* **109**(1098), pp. 373–383.

[4] Hamabe, K., and Ishida, K., 1992. "Rim seal experiments and analysis of a rotor-stator system with non-axisymmetric main flow". In Proceedings of the ASME Turbo Expo, no. 92-GT-160.

[5] Hills, N. J., Chew, J. W., and Turner, A. B., 2002. "Computational and mathematical modelling of turbine rim seal ingestion". *Journal of Turbomachinery (transactions of the ASME),* **124**, pp. 306–315.

[6] Bohn, D., and Wolff, M., 2003. "Improved formulation to determine minimum sealing flow: $c_{w,min}$ - for different sealing configurations". In Proceedings of the ASME Turbo Expo, no. GT2003-38465.

[7] Scanlon, T., Wilkes, J., Bohn, D., and Gentilhomme, O., 2004. "A simple method for estimating ingestion of annulus gas into a turbine rotor-stator cavity in the presence of external pressure variations". In Proceedings of the ASME Turbo Expo, no. GT2004-53097.

[8] Bohn, D., Rudzinski, B., Surken, N., and Gartner, W., 1999. "Influence of rim seal geometry on hot gas ingestion into the upstream cavity of an axial turbine stage". In Proceedings of the ASME Turbo Expo, no. 99-GT-248.

[9] Gentilhomme, O., Hills, N. J., Chew, J. W., and Turner, A. B., 2003. "Measurement and analysis of ingestion through a turbine rim seal". *Journal of Turbomachinery (transactions of the ASME),* **125**, pp. 505–512.

[10] Roy, R. P., Xu, G., Feng, J., and Kang, S., 2001. "Pressure field and main stream gas ingestion in a rotor-stator disc cavity". In Proceedings of the ASME Turbo Expo, no. 2001-GT-564.

[11] Cao, C., Chew, J. W., Millington, P. R., and Hogg, S. I., 2003. "Interaction of rim seal and annulus flows in an axial flow turbine". *Journal of Engineering for Gas Turbines and Power (transactions of the ASME),* **126**, pp. 786–793.

[12] Jakoby, R., Zierer, T., Lindblad, K., Larsson, J., deVito, L., Bohn, D. E., Funcke, J., and Decker, A., 2004. "Numerical simulation of the unsteady flow field in an axial gas turbine rim seal configuration". In Proceedings of the ASME Turbo Expo, no. GT2004-53829.

[13] Roy, R. P., Feng, J., Narzary, D., Saurabh, P., and Paolillo, R. E., 2004. "Experiments on gas ingestion through axial-

flow turbine rim seals". In Proceedings of the ASME Turbo Expo, no. GT2004-53394.
[14] Rosic, B., Denton, J. D., and Pullan, G., 2005. "The importance of shroud leakage modelling in multistage turbine flow calculations". In Proceedings of the ASME Turbo Expo, no. GT2005-68459.
[15] Cherry, D., Wadia, A., Beacock, R., Subramanian, M., and Vitt, P., 2005. "Analytical investigation of a low pressure turbine with and without flowpath endwall gaps, seals and clearance features". In Proceedings of the ASME Turbo Expo, no. GT2005-68492.
[16] Gentilhomme, O. J. P., 2004. "Turbine rim seal ingestion". PhD thesis, University of Sussex.
[17] ROLLS-ROYCE PLC, 2004. *The Hydra user's guide*.
[18] Spalart, P. R., and Allmaras, S. R., 1994. "A one-equation turbulence model for aerodynamic flows". *La Recherche Aerospatiale,* **1**, pp. 5–21.
[19] Batchelor, G. K., 1951. "Note on a class of solutions of the navier-stokes equations representing steady rotationally-symmetric flows". *Quarterly Journal of Mechanics and Applied Mathematics,* **4**, pp. 29–41.
[20] Chavanne, X., Chilla, F., Chabaud, B., Castaing, B., and Hébréal, B., 2001. "Turbulent rayleigh-bénard convection in gaseous and liquid he". *Physics of Fluids,* **13**(5), pp. 1300–1320.